Evolution of modes of Fabry–Perot cavity based on photonic crystal guided-mode resonance mirrors

Pierre Pottier, Lina Shi, and Yves-Alain Peter*

Department of Engineering Physics, Ecole Polytechnique de Montréal, Montréal (QC) H3C 3A7, Canada
**Corresponding author: yves-alain.peter@polymtl.ca*

Received April 11, 2012; revised August 15, 2012; accepted August 15, 2012;
posted August 16, 2012 (Doc. ID 166496); published September 11, 2012

We describe the modes of a Fabry–Perot cavity made of two-dimensional photonic crystal guided-mode resonance mirrors (Si_3N_4 /air), and compare it with an ideal Fabry–Perot cavity and a cavity made of Bragg mirrors. As the evolution of modes is analyzed, a lower tuning efficiency and a larger tuning range are obtained compared to Bragg mirror cavities. New behavior also emerges such as the possibility to tune the inner interface from being a node to an antinode of the standing wave electric field, and therefore the possibility to provide enhancement of emission of nanoemitters binding to the inner interfaces of the cavity, such as in microfluidic microassay systems.

OCIS codes: 230.5298, 230.5750, 120.2230, 230.4040, 030.4070, 230.7408.

1. INTRODUCTION

Fabry–Perot (FP) cavities are a common type of optical resonators and consist of two parallel mirrors separated by a precise distance. The confinement of light provided gives rise to resonances and sharp transmission peaks across the cavity. It is used in particular in spectroscopy and for lasers. Commonly used mirrors are either thin metallic films or distributed Bragg reflectors (DBRs), also known as Bragg mirrors. A particular class of FP based lasers is the vertical cavity surface emitting laser (VCSEL) [1], which provides compactness and a vertical emission compared to its counterparts. The VCSEL is using Bragg mirrors, usually of the order of several tens of alternating different refractive index materials. Other FP configurations may also use an in-plane longitudinal DBR cavity, such as for lasers or sensors [2].

More recently, another way to reflect light has been put into practice. It consists in using guided-mode resonances (GMRs) [3–8], which are obtained using a slab waveguide containing a periodic dielectric pattern, either one-dimensional (1D), like a grating [4], or two-dimensional (2D), like photonic crystals (PhCs) [9]. By a coupling of radiation modes and guided modes, particular transmission features can be achieved. Sharp reflection/transmission peaks can be obtained [10,11], in particular for low filling fractions of the lower index material, or at the opposite wide high-reflection bands can be produced [12,13]; i.e., a mirror is created, usually at higher filling fractions of the lower index material. This relies on a single layer only; therefore very compact devices can be built, such as FP cavities [14–19], with a potential huge quality factor, since the reflectivity of a single-layer PhC GMR mirror can virtually reach 100%. Such high-quality factor and compactness are, among other applications, desired for the enhanced interaction of light with matter such as light enhancement for detection of biological species.

We are interested here in the behavior of this new kind of FP cavity, and the comparison with the other types of FP cavities. Therefore we start in Section 2 by giving the mode characteristics of an ideal FP cavity, and in Section 3 we illustrate the FP cavity made with Bragg mirrors. We describe its characteristics, and discuss the tuning efficiency and tuning range. Thereafter, in Section 4, we address the situation of the FP cavity made with PhC GMR mirrors. Using the finite-difference time-domain (FDTD) method, we calculate the evolution of the transmission peak position versus the gap of the cavity and establish the tuning range and tuning efficiency. We also calculate the distribution of electric field inside the cavity and compare the situation with a Bragg mirror cavity. Then we discuss the modal behavior of the PhC GMR mirror cavity. Finally, in Section 5, we point out applications for biodetection and other possible applications.

2. IDEAL FP CAVITY

Let us first consider the case of an ideal FP cavity. Such a cavity comprises two mirrors separated by a distance g [Fig. 1(a)]. The change of optical phase after one round trip in the cavity is

$$\delta = 2gn_1\frac{2\pi}{\lambda}. \tag{1}$$

This leads to the condition of resonance of the cavity when

$$g = m\frac{\lambda}{2n_1} \tag{2}$$

or

$$\lambda = \frac{2n_1 g}{m}, \tag{3}$$

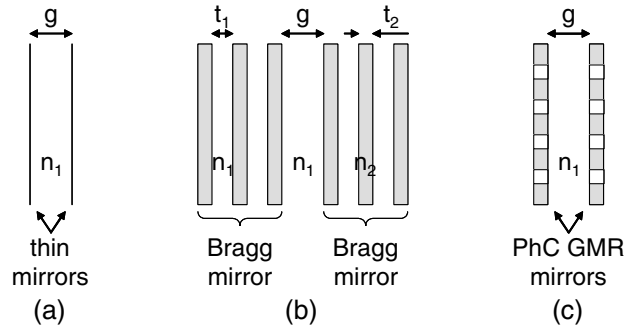

Fig. 1. (a) Schematic of an ideal FP cavity, (b) an FP cavity made of Bragg mirrors, and (c) an FP cavity made of PhC GMR mirrors.

with m an integer, defining the mode of the cavity. We considered the situation where no phase shift occurs upon refection on mirrors. For a cavity made of metallic mirrors, a phase shift of π occurs upon each refection. δ is then increased by 2π and the condition of resonance remains the same. For a given mode m, an ideal FP cavity can be continuously tuned to any wavelength by changing its length g. The resonance wavelength, or transmission peak position, of the cavity is represented in Fig. 2 for modes 1 to 4 ($n_1 = 1$). We use dimensionless cavity length (g/a) and resonance wavelength (λ/a) in order to match with the later PhC situation. a is an arbitrary number (whose quantity is a length) that can be set to provide physical cavity length and wavelength.

3. FP CAVITY WITH BRAGG MIRRORS

Let us now consider the case where two dielectric Bragg mirrors are used as mirrors of the FP cavity [Fig. 1(b)]. The thickness of the elements of index n_2 and the elements of index n_1 is respectively given by

$$t_2 = \frac{(2m_2 + 1)\lambda}{4n_2}, \tag{4}$$

$$t_1 = \frac{(2m_1 + 1)\lambda}{4n_1}, \tag{5}$$

with m_2 and m_1 two integers. With these dimensions the light reflected by each interface of the Bragg mirror is in phase, therefore the reflectivity of the mirrors is maximum and the reflections of the light inside the cavity occur exactly at the inner interfaces of the cavity (separated by the distance g). The phase shift upon refection on mirrors is either 0

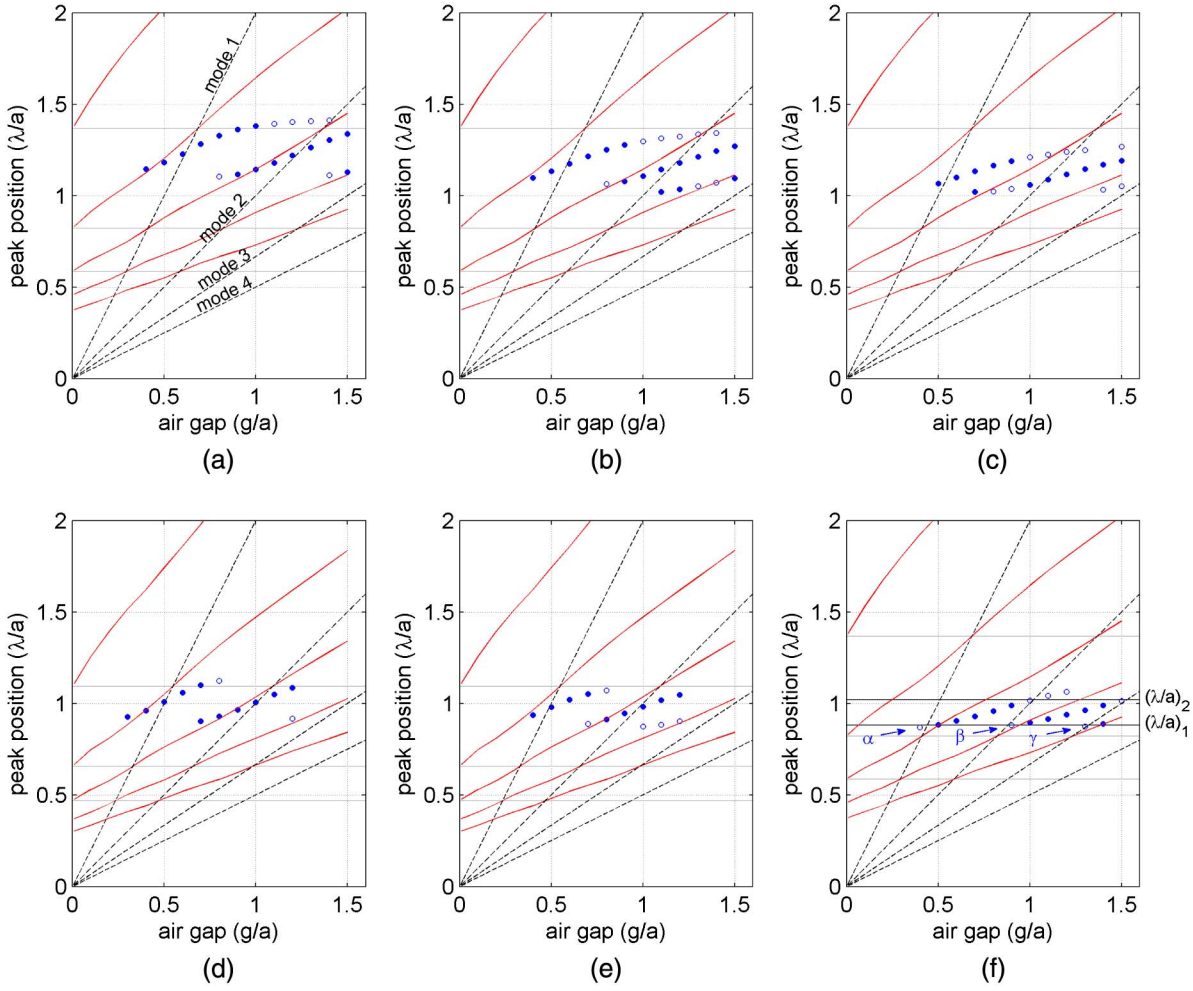

Fig. 2. (Color online) Evolution of modes of an ideal FP cavity (black dashed straight lines), an FP cavity made of Bragg mirrors (red curves), and an FP cavity made of PhC GMR mirrors (dots) for the configurations (a) to (f) in Table 1.

if $n_1 > n_2$ or π if $n_1 < n_2$. Consequently, the condition of resonance is still given by Eq. (2).

If we consider a classical Bragg mirror FP cavity, the Bragg mirrors are frozen; i.e., n_1, n_2, t_1, and t_2 are fixed. Only the separation g can be tuned. But as soon as this distance is changed, the condition (2) or (3) ceases to be true. Indeed, the Bragg mirrors become not optimal for the new resonance wavelength λ and a phase shift occurs upon reflection on them, which changes the phase condition (1), or in other words, the cavity effective length.

In order to estimate the change of resonance wavelength in relation with the gap g, we used a 1D simulation tool based on characteristic matrix approach: Openfilters [20]. The results are displayed in Fig. 2. We reused the dimensionless notation of Section 2. These results are based on one layer of index $n_2 = 2.05$ (with surrounding background $n_1 = 1$) whose dimensionless thickness is $t_2/a = 0.5$ [Figs. 2(a), 2(b), 2(c), and 2(f)] or 0.4 [Figs. 2(d) and 2(e)] in order to be comparable with Section 4 (PhC). Note that we have here a low-quality factor cavity, but our interest is in the position of resonances. As can be seen, the tuning efficiency ($d\lambda/dg$) is lower than for the ideal FP cavity (by roughly a factor of 2).

The positions where the Bragg mirror FP cavity curves intersect the ideal FP cavity curves correspond to the situation where the gap g equals the cavity effective length, i.e., when there is no phase shift, when the Bragg mirrors are in their optimal configuration. This situation (4) corresponds to

$$\frac{\lambda}{a} = \frac{4n_2}{2m_2 + 1}\frac{t_2}{a}. \tag{6}$$

We plotted these horizontal lines in Fig. 2 (in gray) for $m_2 =$ 1 to 3 (different orders of the Bragg mirrors), according to each previously assigned t_2/a value, and validate they cross the aforementioned intersection points. In the vicinity of a straight line corresponding to the mode m of the ideal FP cavity, the Bragg mirror FP cavity behaves properly (high reflectivity of the mirrors). But away from it the reflectivity of the mirrors degrades, down to a point where it reaches zero (when $t_2 = m_3\lambda/(2n_2)$, with m_3 an integer). Therefore, the continuous lines of the Bragg mirror FP cavity go through a situation where there is no effective cavity between two different orders. Such a Bragg mirror FP cavity can then only be tuned over a limited range of wavelengths. The maximum range is the stopband of the Bragg mirror, whose bandwidth is given by [21]

$$\Delta\lambda_0 = \frac{4\lambda_0}{\pi}\arcsin\left(\frac{n_2 - n_1}{n_2 + n_1}\right), \tag{7}$$

with λ_0 the central wavelength. In our situation, when using material/air stacks, $\Delta\lambda_0/\lambda_0 \approx 0.45$. But in common Bragg mirrors, with low index contrast material/material stacks (such as, e.g., GaAs/AlAs), $\Delta\lambda_0/\lambda_0 \approx 0.10$.

4. FP CAVITY WITH PhC GMR MIRRORS

We now investigate the case when the FP cavity is formed by two PhC GMR mirrors [Fig. 1(c)]. The PhC consists of a 2D lattice of circular holes of index $n_1 = 1$ in a material of index $n_2 = 2.05$. The indices n_2 and n_1 correspond to a system of Si_3N_4 material and air, which exhibits advantages such as transparency in the visible range and a significant refractive index contrast. Each PhC slab is used in the situation where a high reflection is obtained over a wide bandwidth, as we previously explored [22,23]. Using a FDTD simulation tool as described in [22], we computed the transmission peak positions of the six configurations of PhC corresponding to the cases (a) to (f) of Fig. 2 in [22], for various separation distances g. These configurations are detailed in Table 1. The results are reported in Fig. 2, with the same numbering of cases (a) to (f). Filled dots correspond to high transmission peaks (> 90%), and empty dots to lower transmission peaks (< 90%).

For each case, all the peaks are contained within a certain wavelength region. This region corresponds to the region of high reflectivity of a single PhC slab (cf. Fig. 2 in [22]), as could be expected. The maximum bandwidth that could be reached is $\Delta\lambda_0/\lambda_0 \approx 0.27$ [22]. Thus the PhC GMR mirror FP cavity has a lower tunable range than the Bragg mirror FP cavity made of the same materials, but it has a higher range than Bragg mirror FP cavities commonly used, such as in VCSEL lasers. And it may possibly still be increased by engineering new designs, e.g., by combining several GMRs. This wide range has the advantage that it can be obtained with a single layer for the mirror, compared to a multilayer for a Bragg mirror. A second advantage is that extremely high-quality factors can potentially be reached, thanks to reflectivities virtually reaching 100%.

We also observe that for all the cases the tuning efficiency ($d\lambda/dg$) is lower than for the ideal FP cavity, and the Bragg mirror FP cavity (by roughly a factor of 2). This reveals the presence of a strong phase shift upon reflection on the PhC GMR mirrors [19,24] because the change of physical path is only partially converted into round-trip phase change. The behavior of a wide reflection PhC GMR mirror, as in our situation, is governed by the coupling of two leaky guided modes of different order [25], which eventually determines the tuning efficiency. A lower tuning efficiency is not usually desired, but its value here is still good to make tunable structures. On the other hand, this leads to an interesting new phenomenon, as we will see below.

Usually, in FP cavities, the inner interfaces are the location of a node of the electric field of the standing wave. This is the case for a metallic mirror FP cavity because the metal imposes a zero electric field at its surface. This is also the case for a dielectric Bragg mirror FP cavity when the cavity material has

Table 1. Lattice Type, Normalized Radius (r/a), and Normalized Thickness (t/a) of Configurations (a) to (f) of Fig. 2 in [22], Reused in Fig. 2 of this Paper

Case	(a)	(b)	(c)	(d)	(e)	(f)
Lattice	Square	Square	Square	Triangular	Triangular	Triangular
r/a	0.35	0.40	0.45	0.30	0.35	0.40
t/a	0.5	0.5	0.5	0.4	0.4	0.5

a lower index than the first Bragg layer. Indeed, in this situation (A), the light acquires a phase shift of π upon reflection, which zeros the electric field. This configuration is the usual one. It happens when the cavity medium is air. It also happens when the cavity medium is water or a biological medium ($n \approx 1.3$), since it will be surrounded by, e.g., glass ($n \approx 1.5$) or a semiconductor ($n \approx 3$). In case of the rarer opposite situation (B), a high-index cavity material with a low-index first Bragg layer, there is a zero phase shift upon reflection, which makes an antinode of the electric field and a node of the magnetic field. A limited phase shift happens in Bragg mirrors, and the Bragg configuration degrades as the cavity length is modified. Therefore, for the usual configuration (A), the inner interface is always close to a node of electric field.

However in the PhC GMR mirror FP cavity, by observing the evolution of distribution of energy in the cavity along the tuning of the gap g, we can see that the inner interface goes from a situation of being a node of the electric field to a situation of becoming an antinode. The distribution of energy (as calculated in [22]) is illustrated in Fig. 3, for the case of Fig. 2(f) and the group of points ranging from dimensionless gap $g/a = 0.9$ to 1.5 and dimensionless wavelength $\lambda/a = 0.88$ to 1.01 (i.e., the middle group β). At $g/a = 1.5$, the inner interface is almost at a node of the electric field and the standing wave comprises three lobes. This position on the graph of Fig. 2(f) is almost on the straight line corresponding to the mode 3 of the ideal FP cavity. As g/a decreases, we observe that the lobes of the standing wave get squeezed down to $g/a = 0.9$, where the inner interface is now almost at an antinode of the electric field. And the standing wave now comprises two lobes. The position on the graph is almost on the straight line corresponding now to mode 2 of the ideal FP cavity. We have gone continuously from the "classical" mode 3 to the "classical" mode 2. But this denomination can no more apply for a PhC GMR mirror FP cavity. A mode of this cavity corresponds now to the line or group of points that we considered in this paragraph (such as α, β, or γ). The mode could potentially contain any number of lobes, as long as the PhC GMR mirror provides a large enough wavelength range of reflectivity. Another mode can be observed at the same gap $g/a = 0.9$, at $\lambda/a = 0.99$ [on the left group of points (α) of Fig. 2(f)] [Fig. 3(h)]. This mode has also two lobes at this position, and is still near the straight line corresponding to mode 2 of the ideal FP cavity. But the inner interface is now almost at a node of the electric field. The positions of nodes and antinodes of electric and magnetic fields have switched compared to the previous mode. Note that we do not reach strictly speaking a node or antinode situation at the inner interfaces, because there will always be the presence of the leaky-guided mode in the PhC slab, but as can be seen in Fig. 3, we get very close to this situation.

On all the graphs of Fig. 2, the lines corresponding to the modes of the PhC GMR mirror FP cavity intersect the straight lines corresponding to the modes of the ideal FP cavity, by groups of identical wavelengths. For example, on Fig. 2(f), this happens at $(\lambda/a)_1 = 0.88$ and $(\lambda/a)_2 = 1.02$. At these intersections, the cavity effective length equals the cavity gap g. The phase shift upon reflection is therefore zero or π. It appears to be zero for $(\lambda/a)_1$ and π for $(\lambda/a)_2$ from the node and antinode positions of Fig. 3. Such a phase shift range

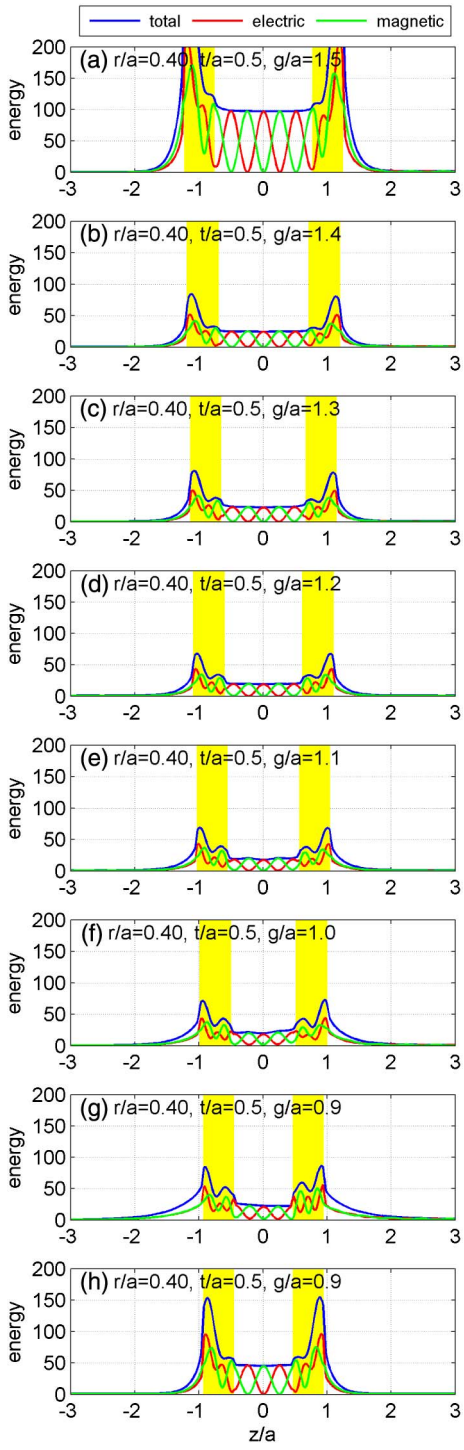

Fig. 3. (Color online) Distribution of energy (as calculated in [22]) [time averaged linear density of electric energy (red curve), magnetic energy (green curve), and total energy (blue curve) along the direction (z) of the cavity] in the PhC GMR FP cavity, for dimensionless gaps $g/a = 0.9$ to 1.5, at their respective resonance wavelength(s). The linear density of total energy of an incident wave is taken as 1. The yellow areas denote positions of the PhC slabs. (a) to (g) correspond to the middle group of points (β) of Fig. 2(f), and (h) to the left group (α).

(more than π) is comparable to the one obtained with higher index material systems [19,24]; however, the choice of shift of zero or π is not necessarily available. In order to verify the phase shift, we also computed the reflection of a single

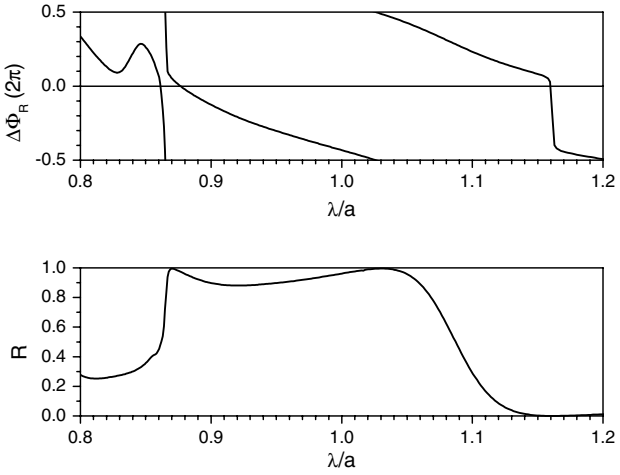

Fig. 4. Phase shift upon reflection $\Delta\Phi_R$ (top) and reflection efficiency R (bottom) of a single PhC GMR mirror [configuration (f) of Table 1] versus dimensionless wavelength (λ/a).

PhC GMR mirror (with FDTD Fullwave software). In Fig. 4 are represented the reflection amplitude and the phase shift upon reflection, i.e., with reference to the first interface of the PhC slab. It can be confirmed that the phase shift is 0 at $(\lambda/a) = 0.876$ and $-\pi$ at $(\lambda/a) = 1.026$, i.e., the dimensionless wavelengths $(\lambda/a)_1$ and $(\lambda/a)_2$ previously mentioned, and that it varies continuously in between, with an overall extent of more than π over the high-reflection region.

Based on these observations, we can predict the wavelengths of the modes of the PhC GMR mirror FP cavity versus the gap g. As a first approximation, we can say that each mode corresponds to the straight line joining the point of intersection of the horizontal line $(\lambda/a)_1$ with the straight line corresponding to the mode m_0 of the ideal FP cavity to the point of intersection of the horizontal line $(\lambda/a)_2$ with the straight line corresponding to the mode $m_0 + 1$ of the ideal FP cavity. This leads to the following straight-line equation:

$$\left(\frac{\lambda}{a}\right) = 2n_1 \frac{(\lambda/a)_2 - (\lambda/a)_1}{(m_0+1)(\lambda/a)_2 - m_0(\lambda/a)_1}\left(\frac{g}{a}\right) + \frac{(\lambda/a)_1(\lambda/a)_2}{(m_0+1)(\lambda/a)_2 - m_0(\lambda/a)_1}. \tag{8}$$

m_0, an integer, thus provides a parameterization of the modes of the PhC GMR mirror FP cavity. These modes exist only in the region where the PhC GMR mirrors have high reflectivity. On the set of cases of Fig. 2, the curves corresponding to the modes are somewhat curved rather than straight lines, so Eq. (8) gives an approximation only, but is still exact at the aforementioned intersections. In Fig. 2(f), the curves are quite straight, so Eq. (8) provides a quite good estimation. The modes of the cavity can be summarized as follows: for a given gap (g/a), the wavelengths $(\lambda/a)_{m_0}$ are given by Eq. (8), and for a given wavelength (λ/a), the gaps $(g/a)_{m_0}$ are given by

$$\left(\frac{g}{a}\right) = \frac{[(m_0+1)(\lambda/a)_2 - m_0(\lambda/a)_1]}{2n_1[(\lambda/a)_2 - (\lambda/a)_1]}\left(\frac{\lambda}{a}\right) - \frac{(\lambda/a)_1(\lambda/a)_2}{2n_1[(\lambda/a)_2 - (\lambda/a)_1]} \tag{9}$$

or

$$\left(\frac{g}{a}\right) = \frac{m_0}{2n_1}\left(\frac{\lambda}{a}\right) + \frac{(\lambda/a)_2\left[\left(\frac{\lambda}{a}\right) - (\lambda/a)_1\right]}{2n_1[(\lambda/a)_2 - (\lambda/a)_1]}. \tag{10}$$

5. APPLICATIONS

Concerning applications in biomolecule detection, FP cavities can be used to enhance the absorption of an element or the emission of a source. The space between the two PhC GMR mirrors could be used as a microfluidic channel for the transport of analytes. For a selective detection, a functionalization of the surface is often sought, and the biomolecules, linked to an optical marker (fluorophore, quantum dot), will adhere to this surface. But the problem with FP cavities made of glass (or semiconductor) to contain a liquid similar to water, or even metalized FP cavities, is that there is no or little electric field at this surface, because it is a node of the standing wave. As a result, the emission will even be damped. On the contrary, with PhC GMR mirror FP cavities, we have shown that it is possible to obtain an antinode of electric field at the inner interface. Therefore it is possible by this way to create an enhancement of emission, potentially very high with the high reflectivity allowed by the mirrors, eventually leading to enhanced sensitivity of detection.

The behavior of PhC slabs as mirrors, using GMR in the high-reflectivity and high-bandwidth regime, allows the creation of very compact FP cavities. It has also been recently proposed to use 1D grating slab mirrors to realize waveguides by trapping the light between two of them [26]. These could also be used with a simple confinement of light in the other direction using classical index contrast, therefore realizing waveguides with lines of posts [Fig. 5(a)] or with 2D PhC strips [Fig. 5(b)]. We can also think at optical fibers that would contain a part of higher index, in the shape of a tube, with a grating in it [Fig. 5(c)], i.e., a periodic change of index, possibly fabricated in a process including an inscription by external or internal exposure. We would therefore have a 1D PhC GMR slab curled on itself, which would allow guiding of light inside, i.e., finally creating a "waveguide in a waveguide." The interaction with the medium inside or around such waveguides can potentially be strong, and a microfluidic channel could in such a way be used to both carry a liquid and to guide light. This could be used for high-sensitivity sensors or for tunability, in particular with an antinode of electric field at the inner

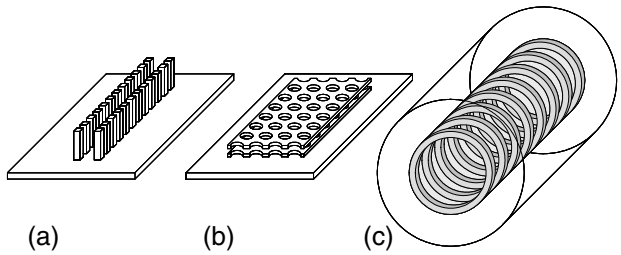

Fig. 5. Optical waveguides using PhC GMR mirrors as the mean of confinement of light. (a) vertical strip waveguide (here with lateral 1D PhC GMR mirrors), (b) horizontal strip waveguide (here with vertical 2D PhC GMR mirrors), and (c) optical fiber circular waveguide (here with circular 1D PhC GMR mirror).

boundaries where optical markers would gather because of functionalization.

6. CONCLUSION

We have presented here a study of cavities that can be built using PhC membranes as mirrors, in the GMR regime, for the Si_3N_4 /air case that is adapted for the visible range and biodetection. We gave a representation of their modal behavior in relation with traditional ideal cavities and cavities using Bragg mirrors. From the analysis of their modes, we have shown that their tuning range is higher than classical Bragg mirror cavities, and can be engineered from the PhC membrane design. Additionally, their tuning efficiency is lower than classical Bragg mirror cavities, in relation with a strong phase shift on reflection. This effect is also at the origin of a different energy distribution inside the cavity, with a varying number of lobes of electric field, and high or low presence of electric field at the inner interfaces. These effects can be put to advantage for the enhancement of nanoparticule emission, as well as for laser control and optical filters, and also for new guiding devices.

ACKNOWLEDGMENTS

This work was supported by the Natural Sciences and Engineering Research Council of Canada (NSERC), Strategic Grant 336830-2006. P. Pottier would like to thank M. Packirisamy from Concordia University for Fullwave computing resources.

REFERENCES

1. K. Iga, S. Kinoshita, and F. Koyama, "Microcavity GaAlAs/GaAs surface-emitting laser with $I_{th} = 6$ mA," Electron. Lett. **23**, 134–136 (1987).
2. R. St-Gelais, A. Poulin, and Y.-A. Peter, "Advances in modeling, design, and fabrication of deep-etched multilayer resonators," J. Lightwave Technol. **30**, 1900–1908 (2012).
3. R. W. Wood, "On a remarkable case of uneven distribution of light in a diffraction grating spectrum," Proc. Phys. Soc. London **18**, 269–275 (1902).
4. A. Hessel and A. A. Oliner, "A new theory of Wood's anomalies on optical gratings," Appl. Opt. **4**, 1275–1297 (1965).
5. M. Nevière, "The homogeneous problem," in *Electromagnetic Theory of Gratings*, R. Petit, ed. (Springer-Verlag, 1980), pp. 123–157.
6. V. N. Astratov, D. M. Whittaker, I. S. Culshaw, R. M. Stevenson, M. S. Skolnick, T. F. Krauss, and R. M. De La Rue, "Photonic band-structure effects in the reflectivity of periodically patterned waveguides," Phys. Rev. B **60**, R16255–R16258 (1999).
7. S. Fan and J. D. Joannopoulos, "Analysis of guided resonances in photonic crystal slabs," Phys. Rev. B **65**, 235112 (2002).
8. K. B. Crozier, V. Lousse, O. Kilic, S. Kim, S. Fan, and O. Solgaard, "Air-bridged photonic crystal slabs at visible and near-infrared wavelengths," Phys. Rev. B **73**, 115126 (2006).
9. S. Peng and G. M. Morris, "Experimental demonstration of resonant anomalies in diffraction from two-dimensional gratings," Opt. Lett. **21**, 549–551 (1996).
10. R. Magnusson and S. S. Wang, "New principle for optical filters," Appl. Phys. Lett. **61**, 1022–1024 (1992).
11. S. Tibuleac and R. Magnusson, "Reflection and transmission guided-mode resonance filters," J. Opt. Soc. Am. A **14**, 1617–1626 (1997).
12. C. F. R. Mateus, M. C. Y. Huang, L. Chen, C. J. Chang-Hasnain, and Y. Suzuki, "Broad-band mirror (1.12–1.62 μm) using a subwavelength grating," IEEE Photonics Technol. Lett. **16**, 1676–1678 (2004).
13. O. Kilic, S. Kim, W. Suh, Y.-A. Peter, A. S. Sudbø, M. F. Yanik, S. Fan, and O. Solgaard, "Photonic crystal slabs demonstrating strong broadband suppression of transmission in the presence of disorders," Opt. Lett. **29**, 2782–2784 (2004).
14. W. Suh, M. F. Yanik, O. Solgaard, and S. Fan, "Displacement-sensitive photonic crystal structures based on guided resonance in photonic crystal slabs," Appl. Phys. Lett. **82**, 1999–2001 (2003).
15. S. Boutami, B. Benbakir, X. Letartre, J. L. Leclercq, P. Regreny, and P. Viktorovitch, "Ultimate vertical Fabry-Perot cavity based on single-layer photonic crystal mirrors," Opt. Express **15**, 12443–12449 (2007).
16. M. C. Y. Huang, Y. Zhou, and C. J. Chang-Hasnain, "A surface-emitting laser incorporating a high-index-contrast subwavelength grating," Nat. Photonics **1**, 119–122 (2007).
17. H. Y. Song, S. Kim, and R. Magnusson, "Tunable guided-mode resonances in coupled gratings," Opt. Express **17**, 23544–23555 (2009).
18. T. Stomeo, M. Grande, G. Rainò, A. Passaseo, A. D'Orazio, R. Cingolani, A. Locatelli, D. Modotto, C. De Angelis, and M. De Vittorio, "Optical filter based on two coupled PhC GaAs-membranes," Opt. Lett. **35**, 411–413 (2010).
19. D. Zhao, Z. Ma, and W. Zhou, "Field penetrations in photonic crystal Fano reflectors," Opt. Express **18**, 14152–14158 (2010).
20. S. Larouche and L. Martinu, "OpenFilters: open-source software for the design, optimization, and synthesis of optical Filters," Appl. Opt. **47**, C219–C230 (2008).
21. P. Yeh, *Optical Waves in Layered Media* (Wiley, 1988), pp. 144–165.
22. L. Shi, P. Pottier, M. Skorobogatiy, and Y.-A. Peter, "Tunable structures comprising two photonic crystal slabs—optical study in view of multi-analyte enhanced detection," Opt. Express **17**, 10623–10632 (2009).
23. P. Pottier, L. Shi, and Y.-A. Peter, "Determination of guided-mode resonances in photonic crystal slabs," J. Opt. Soc. Am. B **29**, 109–117 (2012).
24. J. H. (E.) Kim, L. Chrostowski, E. Bisaillon, and D. V. Plant, "DBR, Sub-wavelength grating, and Photonic crystal slab Fabry-Perot cavity design using phase analysis by FDTD," Opt. Express **15**, 10330–10339 (2007).
25. S. Boutami, B. Ben Bakir, H. Hattori, X. Letartre, J.-L. Leclercq, P. Rojo-Romeo, M. Garrigues, C. Seassal, and P. Viktorovitch, "Broadband and compact 2-D photonic crystal reflectors with controllable polarization dependence," IEEE Photonics Technol. Lett. **18**, 835–837 (2006).
26. Y. Zhou, V. Karagodsky, B. Pesala, F. G. Sedgwick, and C. J. Chang-Hasnain, "A novel ultra-low loss hollow-core waveguide using subwavelength high-contrast gratings," Opt. Express **17**, 1508–1517 (2009).